Strauch [Beeskow-Strauch], B., Schicks, J., Luzi-Helbing, M., Naumann, R., Herbst, M. (2018): The Difference between Aspired and Acquired Hydrate Volumes -A Laboratory Study of THF Hydrate Formation in Dependence on Initial THF:H 2 O Ratios. - *Journal of Chemical Thermodynamics*, *117*, pp. 193—204.

DOI: http://doi.org/10.1016/j.jct.2017.09.013

The Difference between Aspired and Acquired Hydrate Volumes -

A Laboratory Study of THF Hydrate Formation in Dependence on Initial THF:H_2O Ratios

Bettina Strauch[1], Judith M. Schicks[1], Manja Luzi-Helbing[1], Rudolf Naumann[1], Marcel Herbst[2]

[1] GFZ German Research Centre for Geosciences, Telegrafenberg, 14473 Potsdam, Germany

[2] Freie Universität Berlin, Takustrasse 3, 14195 Berlin, Germany

Keywords: Clathrate hydrates, THF, tetrahydrofuran, calorimetry, Raman spectroscopy

Abstract

The study reports on the differences between theoretically expected and effectively obtained volume fractions of THF hydrate depending on the THF-H_2O ratio in the initial solution against the background of using it as a substitute for natural hydrate in laboratory simulations. Besides the stoichiometric solution, initial solutions with either H_2O or THF as excess phase were prepared to define the wanted volume of hydrate in advance. In order to achieve a chemical equilibrium a complete conversion of H_2O and THF into THF hydrate and the presence of a pure excess phase is impossible. Based on the specific enthalpy of hydrate- and ice melting gained from calorimetric measurements, considerably lower than expected hydrate volumes are concluded. For the stoichiometric solution, containing 19.1 Wt% THF, enthalpy recalculations and the occurrence of an ice melting endotherm indicate incomplete conversion with a residual of 4.3 Vol% unconverted THF-H_2O solution. The deviations from expectations increase with decreasing amount of aspired THF hydrate saturation and are stronger when formed from H_2O excess solutions with up to 25 Vol% less hydrate than projected for full conversion. THF-rich solutions form hydrate with melting enthalpies that recalculate for up to 15 Vol% hydrate less than theoretical assumptions.

In samples with initial THF concentrations below 5 Wt% and above 82.7 Wt% no hydrate formation was evident.

Based on the results we propose corrections to the initial solutions when defined THF hydrate volumes are required. Furthermore, THF excess and temperatures below zero assure stable conditions for hydrate-liquid setting at atmospheric pressure.

1. INTRODUCTION

Tetrahydrofuran (C_4H_8O, THF) is a colorless organic liquid and belongs to the chemical compounds of cyclic ethers [1]. Due to its polar molecular structure it is fully H_2O -miscible. It forms a clathrate hydrate, an ice-like crystalline solid composed of a three-dimensional network of hydrogen-bonded H_2O molecules that confines THF as guest molecule in the hexakaidecahedra ($5^{12}6^4$) of structure II hydrates [2]. Since THF hydrate dissociates into H_2O and THF as liquid phase, THF hydrate it is strictly speaking defined as a liquid hydrate in contrast to a gas hydrate such as CH_4 hydrate dissociating into a gas phase and a liquid aqueous phase [3].

Despite the differences to CH_4 molecules in terms of size, polarity and hence hydrate guest characteristics, THF presents important advantages for studying hydrate characteristics via laboratory simulations. Whilst light hydrocarbons are only slightly soluble in H_2O and hydrate formation therefore requires elevated pressure, THF is well miscible with H_2O and hydrate forms already at moderate temperature and pressure conditions ($\leq$ 277 K and 0.1 MPa). Since it is possible to mix THF and H_2O in any proportions, a defined hydrate saturation in the sediment pore space can be well defined in advance simply by applying the relevant THF- H_2O ratio. This facilitates the synthesis of well-characterized hydrate-bearing sediment specimens and allows the reproduction of typical hydrate reservoir situations. Especially for the investigation of the influence of the degree of hydrate saturation in the pore space on geo-mechanical and geophysical properties of the sediment body, these simulations have long been used for laboratory studies.

Lee et al. investigated the suitability of THF hydrates as replacement for CH_4 hydrates for studies of hydrate bearing sediments. They concluded that THF hydrate – despite the differences

between THF and CH_4 hydrates – can be used as substitute for CH_4 hydrate for macroscopic scale laboratory studies [4]. The effects of sediment matrix to the thermal properties of THF hydrate were observed by Rueff and Sloan [5]. The study shows no noticable changes of the hydrate characteristic when granular sediment is present. Pearson et al. used THF hydrate to perform acoustic and resistivity measurements on rock samples as analogues for natural gas hydrate deposits [6]. For the formation of the THF hydrate they used a THF-H_2O mixture with a THF-H_2O ratio of 1:18 assuming a complete hydrate saturation of the sample. With the addition of 0.05-0.1 M NaCl they varied the amount of unfrozen H_2O and affected the formation of THF hydrate. Yun et al. determined the compressional and shear wave velocities of hydrate-bearing sand. They varied the composition of the THF-H_2O mixtures to achieve hydrate saturations between 43% and 100% of the pore space [7]. In another study Yun et al. determined the mechanical properties of sand, silt, and clay containing THF hydrate [8]. In this study they only used three THF-H_2O mixtures to realize two different hydrate saturations of the pore space. Similar to the first study they combined 80.9 Wt% H_2O and 19.1 Wt% THF for 100% hydrate saturation. Samples with 50% hydrate-filled porosity were obtained by mixing either 90.6 Wt% H_2O and 9.4 Wt% THF or 42.2 Wt% H_2O and 57.8 Wt% THF. The first mixture produces H_2O in excess, the latter THF in excess. Rydzy et al. as well as Priegnitz et al. obtained different hydrate saturations with various THF-H_2O mixtures in order to study physical properties of hydrate bearing sediments as a function of hydrate saturation [9,10]. In any case, the supposed amounts of hydrates can only be formed, when all of the THF (or H_2O) will be transferred into the hydrate.

Corrections due to incomplete formation due to chemical equilibrium have not been considered. The stoichiometric composition of THF hydrate is 1THF : 17H_2O, which equals a

ratio of 19.1 Wt% THF : 80.9 Wt% H_2O. However, the hydrate formation from H_2O and THF is not complete. As seen in the THF- H_2O phase diagram, THF hydrate coexists at equilibrium conditions with a liquid or solid phase that contains a defined amount of THF and H_2O [11]. In any case it is uncertain, if the equilibrium state is reached when THF hydrate is prepared for laboratory studies.

Different studies were carried out to determine the properties of THF hydrates, such as the enthalpies of decomposition and heat capacities [12,13], the stability fields of the THF-H_2O system at low pressures [14], the effect of sediments on the stability boundaries [5,15], and the molecular interactions between the THF guest molecules and the H_2O host molecules in the hydrate structure [16,17]. Also, THF hydrate has been widely investigated in terms of its kinetic and thermophysical properties [18,19,20,21]. The first data on THF hydrate arise from the PhD study of Palmer [22]. He investigated various compounds for the hydrate formation capabiltiy and published a range of THF hydrate formation temperature and phase diagrams showing the phase boundary of various mixtures of THF and H_2O. He noted that the eutectic temperature is not definitely to state, because the temperature around the eutectic is like a plateu in the range of 6 and 8 mol% THF without the formation of a definite turning point. Following this first work, Erva published freezing points of thirty-six different THF-H_2O mixtures at ambient pressures [23]. He observed a congruent melting of the mixture with an approximate composition of C_4H_8O . 16 H_2O (6 mol%) at 277.38 K. Adding H_2O to this composition makes a eutectic system with a eutectic melting point of 272 K and an eutectic mixture containing 0.9 mol% THF. Adding THF to this composition up to 30 mol% THF causes a system with incongruent hydrate melting above 273 K. Thorpe and Pinder obtained seventy-five melting points at concentrations between zero and 20 mol% THF by analysing the refractive index of the soultions [24]. They

also observed defined breaks in the melting point curve and postulate that in a melting hydrate slurry exists a small amount of crystalline hydrate plus a certain amount of two liquid complexes corresponding to the upper and lower hydrogen bonded states.

To simulate certain hydrate saturations, defined volumes of hydrate are necessary. While 17 mol of H_2O react with 1 mol THF to the stoichiometric THF hydrate, a well calculated excess phase of either H_2O or THF is applied to get the desired experimental hydrate:liquid ratios:

$$17\ H_2O + 1\ THF \rightleftharpoons 1\ THF\ hydrate$$

$$17\ (+\ Excess)\ H_2O + 1\ THF \rightleftharpoons 1\ THF\ hydrate + Excess\ H_2O$$

$$17\ H_2O + 1\ (+\ Excess)\ THF \rightleftharpoons 1\ THF\ hydrate + Excess\ THF$$

Thereby, aspects of phase equilibrium are commonly neglected. One prerequisite to reach a phase equilibrium between coexisting liquid and crystalline hydrate phases is fulfilled when there is no difference between the chemical potential in both phases. In a chemical equilibrium between the THF hydrate phase and the coexisting aqueous solution, a certain amount of THF will therefore remain in the aqueous solution and cannot be transferred into the hydrate phase. The same applies for the mixtures using THF in excess. Here, not all H_2O can be transferred into the hydrate phase but some H_2O will remain in the coexisting liquid phase. In addition, it is uncertain, if the equilibrium state is generally reached when THF hydrate is prepared for laboratory studies. Therefore, the reaction of H_2O and THF to form THF hydrate is likely incomplete even if stoichiometric ratios are used in the initial solution.

By using calorimetry we determined the amount of coexisting phases by calculating the specific heat of the components in the mixture upon warming to conclude on the amount of existing hydrate phase in the mixed system. Furthermore, we applied Raman spectroscopic

measurements to determine the THF concentration in the coexisting aqueous phase and the THF-H_2O ratio in the hydrate phase depending on the THF concentration in the initial solution.

The objective of this work is to study THF- H_2O mixtures in the range from 0 to 100 Vol% of expected hydrate saturation, with respect of the degree of completeness of hydrate formation and composition of the excess THF- or H_2O-rich solution.

2. EXPERIMENTAL METHODS

2.1. Preparation of THF-H_2O mixtures of defined compositions

For the preparation of THF-H_2O-mixtures tetrahydrofuran (purity ≥ 99.9 %, Carl Roth GmbH + Co. KG (Karlsruhe, Germany)) and purified deionized H_2O were used. The mixtures were prepared in glass or Teflon flasks. The standard uncertainty for the preparation process is ±0.01Wt%.

Table 1. Properties and supplier of material

Material	**Purity**	**Supplier / System**
THF	≥ 99.9 % (stated by supplier)	Carl Roth GmbH + Co. KG (Karlsruhe, Germany)
deionized H_2O	Total Organic Carbon <20 ppb, ≤ 0.055 µS/cm; 18.2 MΩ-cm (system conductivity analysis)	Evoqua LLC / Seralpur Pro 90 CN

Defining the ratio of THF and H_2O in the initial solution shall provide an accurate hydrate saturation in the final test specimen. Assuming all THF will be transferred into a hydrate phase, THF hydrate saturation of 100 Vol% is reached when 80.9 Wt% H_2O is combined with 19.1 Wt% THF by mass. Specimens with 50 Vol% hydrate-filled pore space are obtained by mixing either 90.6 Wt% H_2O and 9.4 Wt% THF (produces excess H_2O) or 42.2 Wt% H_2O and 57.8 Wt% THF (produces excess THF).

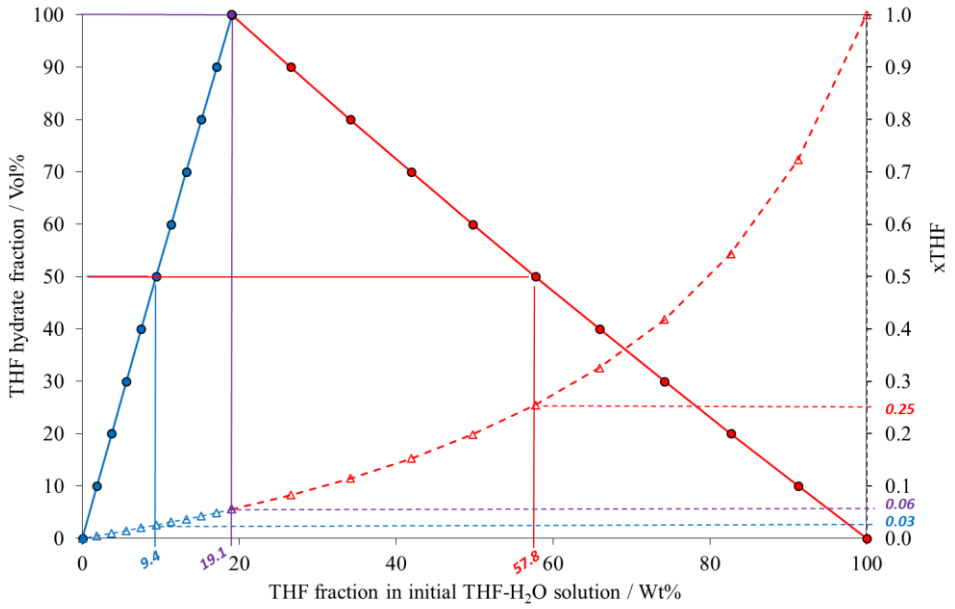

Figure 1. Solid lines: Expected THF hydrate fraction in dependency of THF fraction in the initial THF-H_2O solution. Also shown on the right axis is the mol fraction of THF in the respective initial solutions (dotted lines). Blue colored symbols and lines indicate the H_2O-rich system, red colored marks present the system with an excess of THF. The 100% hydrate fraction is shown in violet.

For experimental simulation utilizing defined hydrate saturations, the volumetric part of THF hydrate that occupies the pore space is of interest rather than the mass percentage. On the other hand, in our experience, sample preparation is easily and fast done by weighting the reactants into the reaction vessels. Therefore, a conversion of Wt% into Vol% is necessary to relate the

THF:H_2O mixing ratios to the desired Vol% that is occupying pore space. Figure 1 illustrates the stoichiometric correlation between THF concentration in the initial solution and the hydrate fraction in the product. It shows that for a full conversion of the THF-H_2O solution into hydrate 19.1 Wt% THF must exist in the initial solution, which equals 0.06 mol fractions of THF. To form a sample with a THF hydrate fraction of 50 Vol%, the THF concentration in the initial solution has to be either 9.4 Wt% or 57.8 Wt% which equals a mol fraction of 0.03 and 0.25 THF, respectively. Beside the 50 Vol% hydrate fraction, 50 Vol% H_2O or THF are present.

Table 2. Basics for the calculation of the volumetric hydrate ratio in the sample. Density values for H_2O and THF have been obtained from [25] and [26], respectively. The density of THF hydrate has been calculated based on [2], ambient pressure is assumed.

stoichometric ratio							
m / g / mol	*18.01*		*72.11*		*378.37*		
	H_2O	**+**	**THF**	**→**	**Hydrate**		
n / mol	17.00		1.00		1.00		
mol%	0.94		0.06		1.00		
Weight / g	306.26		72.11		378.37		
Wt%	**80.94**		**19.06**		100.00		
Density / g/cm³	0.998		0.889		0.970		
Volume / cm³	306.81		81.09		390.07		
Vol%	79.10		20.90		**100**		
Excess THF							
	H_2O	**+**	**THF**	**→**	**Hydrate**	**+**	**THF (l)**
n / mol	17.00		5.81		1.00		4.81
mol%	0.75		0.25		0.17		0.83
Weight / g	306.26		418.88		378.37		346.77
Wt%	**42.23**		**57.77**		52.18		47.82
Density / g/cm³	0.998		0.889		0.97		0.889
Volume /cm³	306.81		471.18		390.07		390.07
Vol%	39.44		60.56		**50**		**50**
Excess H_2O							
	H_2O	**+**	**THF**	**→**	**Hydrate**	**+**	**H_2O (l)**
n / mol	38.62		1.00		1.00		21.62
mol%	0.97		0.03		0.04		0.96

Weight / g	695.55	72.11	378.37	389.29
Wt%	**90.61**	**9.39**	49.29	50.71
Density / g/cm³	0.998	0.889	0.970	0.998
Volume / cm³	696.94	81.11	390.07	390.07
Vol%	89.57	10.43	**50**	**50**

The basics for the calculation of THF hydrate fractions are given in table 1. Exemplarily, the calculation of a solution is shown, where a sample of 50 Vol% THF hydrate content is intended to form. The hydrate content can either be reached by preparing a THF-rich solution or by preparing a solution with H_2O in excess. The density of H_2O and THF is well known, the density of THF hydrate has been calculated by the formula according Sloan and Koh [2].

All of the above described calculations assume a full conversion of all available THF and H_2O into hydrate phase and the presence of excess phase containing only one pure component (H_2O or THF). Aspects of chemical equilibrium are here disregarded.

2.2. Calorimetric measurements

For the calorimetric measurements a BT 2.15 from SETARAM was used. The system consists of a calorimetric chamber, electrical and pneumatic peripherals and a liquid nitrogen supply. The calibration of the system has been performed using melting events of Hg standard and H_2O. Subsequent to cooling, a slow heating rate of 0.02 K/min was applied for accurate detection of the melting. All samples were analyzed in stainless steel cells.

For the study presented here, approximately 0.5 g of the freshly prepared THF-H_2O initial solution was weighted into the vessel, closed with an O-ring sealed lid and introduced into the calorimetric chamber. The reference vessel was kept empty. The calorimetric block was flushed with helium and held at low pressure of about 0.02 MPa for cooling. Upon heating, a similarly

low-pressure nitrogen gas was applied to ensure a high quality heat signal. For cooling, liquid nitrogen was supplied from an external 100 L tank. The liquid nitrogen level in the calorimeter was kept constant through an automatic controlling system which regulates the inflow using a solenoid valve.

First, rapid cooling (0.5 K/min) from ambient temperature to 233 K was performed within 150 min to allow for the total crystallization of the sample (Fig. 2). This was followed by a fast increase to 263 K. To obtain clear, high-quality signals of onset and offset of ice melting and THF hydrate dissociation and the corresponding heat flow during these phase changes, the heating rate was reduced to 0.02 K per minute in the temperature range of 263 to 283 K. The low heating rate was chosen to avoid blurred boundaries of the close-by melting events of ice and THF hydrate. At 283 K the sample was rapidly heated to ambient temperature.

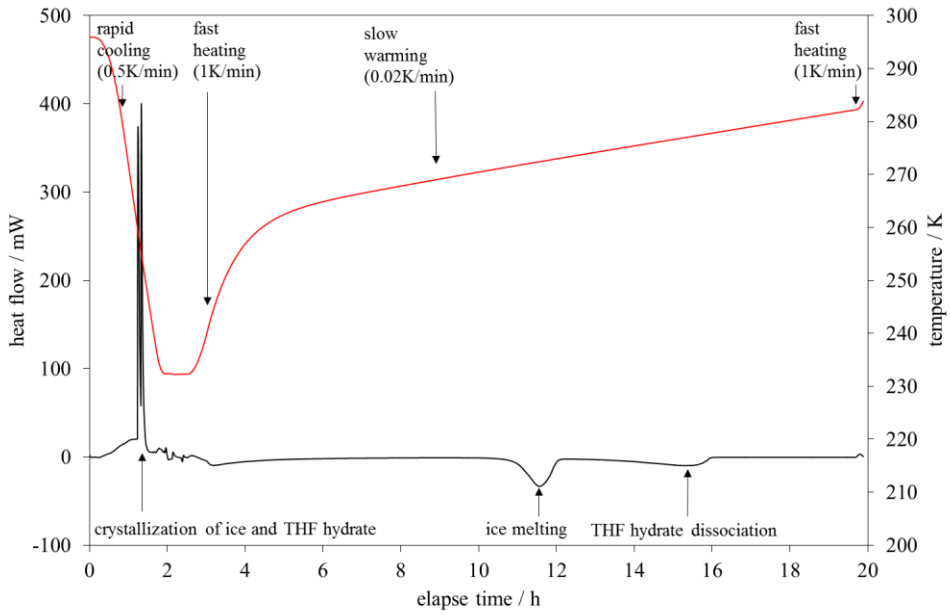

Figure 2. Temperature program and thermogram of a typical calorimetric measurement. The red line shows the cooling and heating regime during the experiment, the black line represents the corresponding heat flow signals with crystallization and melting events for a THF-H_2O sample with H_2O in excess.

Due to the time- and liquid N_2 consuming process of lowering the temperature, only for few samples cooling was extended to 133 K, to achieve data of temperature and enthalpy for THF crystallization and melting. The beginning and end of ice melting and hydrate dissociation are marked by the first and last deviation of the measuring curve from the baseline. These values are not reproducible, therefore we determined the on- and offset temperatures of these processes. For the determination of the on- and offset temperature of a phase transition in a calorimetric curve, the inflectional tangent at the ascending peak slope is extended until it intersects the extrapolated initial baseline. The crossing marks the on- and offset temperature. The determination of on- and offset temperatures as well as the enthalpy are described in more detail in Rydzy et al. [27].

2.3. Raman spectroscopic measurements

Raman spectra were taken using a confocal Raman spectrometer (LABRAM, HORIBA JOBIN YVON). Each sample was analyzed three times (used instrument parameters: grating: 1800 grooves/mm, entrance slit: 100 µm, confocal pinhole: 500 µm, microscope objective: 20x, laser: external 100 mW diode-pumped solid-state laser with a wavelength of 532 nm). The Raman instrument was calibrated using silicium (521 cm^{-1}).

For the preparation of the hydrate phase coexisting besides an aqueous phase, the THF-H_2O mixtures were cooled to 263 K. After the formation of a solid phase (THF hydrate and ice) the samples were warmed in a cooling box to 273.65 K or 275.15 K until the ice phase melted and the hydrate phase besides a coexisting aqueous phase remained. In the case we used excess THF the THF hydrate formed besides a THF-rich liquid phase (no ice phase). For the measurement of the hydrate phase 2-3 hydrate crystals of each hydrate sample were transferred into a cooled

Linkam cooling stage (243 K). At least three spectra at different areas of the crystals were taken. For the measurements of the coexisting aqueous phase (THF-H_2O mixtures) 3-4 samples were taken from the liquid phase of each mixture and transferred into a cooled sample cell (283.15 K) to analyze each sample three times with Raman spectroscopy. To determine the calibration curve a similar procedure was applied.

3. RESULTS AND DISCUSSION

3.1. Calorimetry

The experimental results of the calorimetric measurements are summarized in Table 3. Experimental results of calorimetric measurements. The uncertainties were calculated based on 2-4 replicates. For these, the complete procedure of analysis - from sample preparation over measurement to data evaluation has been repeated.

Table 3. Experimental results of calorimetric measurements.

Excess phase	THF in initial solution	onset temp ice melting	offset temp ice melting	enthalpy melting ice	onset temp hyd melting	offset temp hyd melting	enthalpy hyd melting	onset temp THF melting	offset temp THF melting	enthalpy THF melting
	Wt%	K	K	J/g	K	K	J/g	K	K	J/g
standard uncertainties	± 0.01	± 0.1	± 0.2	± 11.3	± 0.3	± 0.3	± 10.8	± 0.1	± 0.1	± 4.5
H_2O	0.0	273.4	274.7	337.2						
H_2O	2.3	272.0	273.5	320.4						
H_2O	4.5	272.0	273.4	308.7						
H_2O	6.7	272.0	273.2	254.9	275.3	275.9	9.9			
H_2O	8.7	271.9	273.1	206.9	275.5	276.4	30.5			
H_2O	9.4	271.9	273.1	193.3	275.6	276.9	51.3			

H_2O	10.7	271.9	273.0	166.0	275.8	277.5	74.6			
H_2O	12.4	271.8	272.9	132.7	276.0	278.0	107.0			
H_2O	14.3	271.8	272.8	101.5	276.1	278.5	137.1			
H_2O	15.9	271.8	272.6		276.3	278.6				
H_2O	17.8	271.8	272.5	33.1	276.8	278.8	219.0			
none	19.1	271.7	272.2	21.4	277.0	278.7	238.0			
none	19.2				277.1	278.7	254.3			
THF	26.1				276.9	278.7	223.8			
THF	34.5				276.0	278.1	175.1			
THF	42.6				275.9	277.5	145.4	163.4	165.0	32.7
THF	49.0				274.9	276.7	131.7			
THF	57.3				274.2	276.2	92.2	163.5	165.4	54.6
THF	65.6				273.8	275.9	60.2			
THF	74.5				272.0	276.0	30.6	163.6	165.9	82.1
THF	82.6				266.7	277.3	9.1	163.5	165.9	92.1
THF	100.0							163.4	165.0	113.0

3.1.1. Occurrence of phase changes

Hydrate and ice formation from H_2O-rich samples need a certain degree of undercooling to occur in a practical time frame. By cooling to 243 K, crystallization of both was assured. Ice and hydrate crystallization mostly appears in form of two sharp exothermic peaks, usually in a temperature range of 270 K to 245 K (Fig. 3). They crystallize spontaneously with a large heat release within a short time and a distinct peak shape with a linear rising front and a subsequent gently declining curve progression. The peak areas vary depending on the THF concentration in the initial solution. The higher the THF concentration in the initial solution the larger the exothermic peak areas of THF hydrate during crystallization. Corresponding to that, the peak area of ice crystallization decreases. The hydrate and ice crystallization takes place in a fairly random manner from the bulk supercooled solution (Fig. 3).

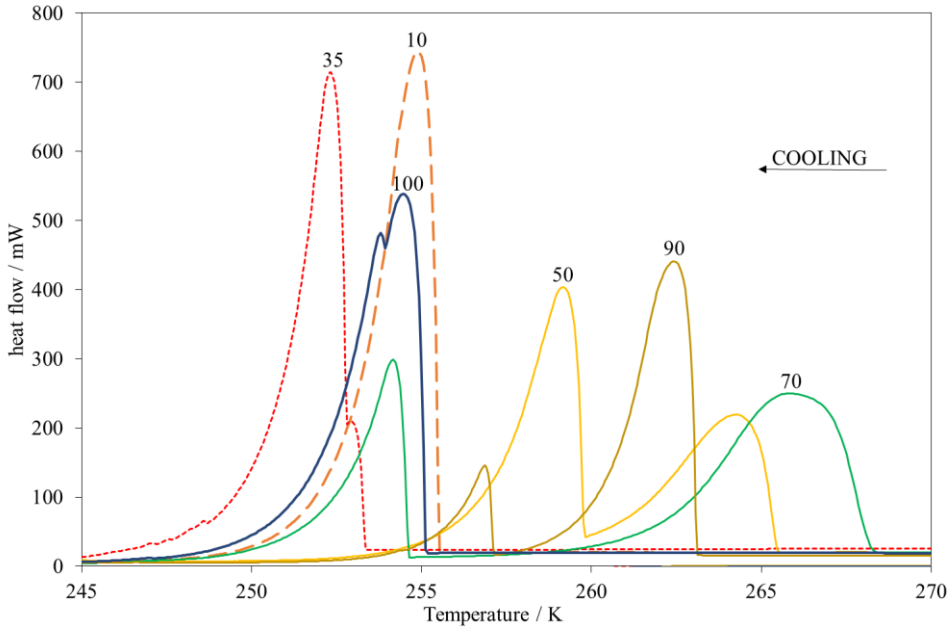

Figure 3. The appearance of exotherms caused by ice and hydrate crystallization. The peaks are labeled with the amount of expected hydrate in Vol%.

The determination of peak occurrence on crystallization of approximately 50 different THF-H_2O mixtures shows variable peak positions and also an inhomogeneity in the occurrence of either one or two exotherms. Observations from temperatures of peak arising in dependence of THF:H_2O ratios indicate, that with increasing THF content, an individual exothermic peak occurs that increases in size while the second one at lower temperature decreases in size. The observation indicates, that THF hydrate crystallizes first and is followed by the formation of ice. This finding is in agreement with Tombari et al. [28]. However, it is noteworthy that THF hydrate formation and ice crystallization occur not necessarily separately. In our studies identical THF-H_2O solutions have been observed to produce one exotherm in one experiment and two exotherms in another. This appears to follow no system and indicates that THF hydrate and ice formation occurs either separately, one after the other, or can also be simultaneously.

Even though there must be a certain amount of THF not incorporated in the hydrate phase upon its formation, cooling to 133 K (below THF crystallization at 164.75 K) [1] did not cause a further exothermic peak to appear. We conclude that unconverted THF does not constitute a distinct liquid phase after ice and hydrate crystallizations but is incorporated in the ice phase. The crystallized ice phase is therefore considered to be to some degree contaminated with THF.

Generally, the exotherms of crystallization are regarded as unreliable in terms of time and temperature of occurrence for comparable studies on hydrate characteristics or contents and are therefore not discussed in further detail.

Upon warming the solid sample, ice melting was observed first followed by hydrate melting above 273.15 K (Fig. 4). The areas and the onset and offset temperature of the endotherms vary systematically depending on the concentration of the respective phases. Notably is the merging of endotherms with decreasing THF content. Hydrate dissociation was observed at THF concentrations higher than 6.7 Wt% in the initial solution (approx. 35 Vol% expected hydrate) with the hydrate melting event closely attached to the ice melting (Fig. 4). It is likely that below these concentrations no hydrate is present which is in agreement the THF-H_2O phase diagrams available in the literature which show varying eutectic compositions for the THF-H_2O system between 3.6 Wt% and 9 Wt% [11,14,29].

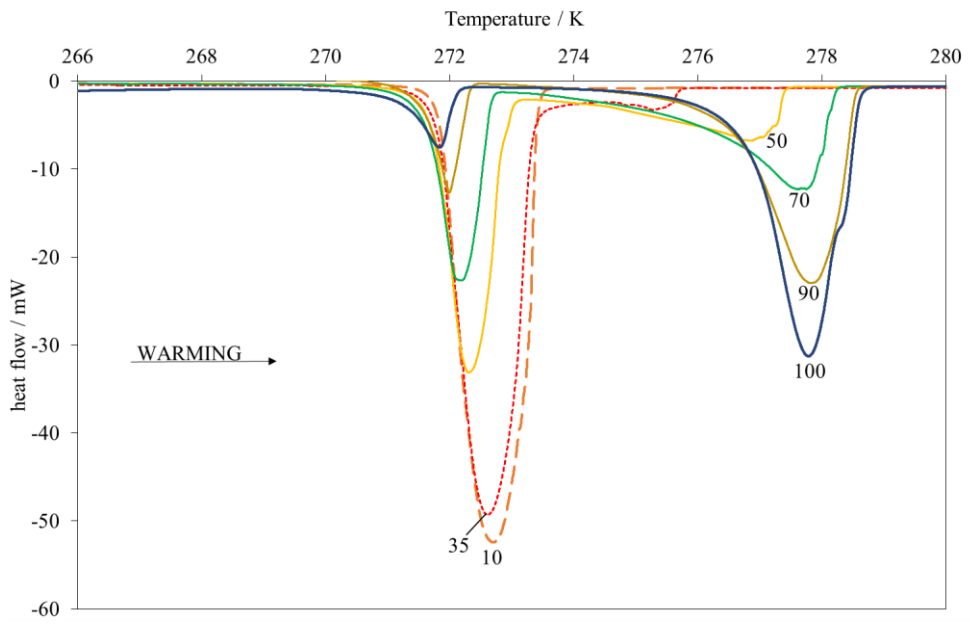

Figure 4. Two endothermic peaks around 272 K and 277 K indicate ice melting and THF hydrate dissociation, respectively. The values on the graphs indicate the expected THF hydrate concentration in Vol%.

In samples containing THF in excess, only one exotherm has been observed at temperatures around 260 K indicative for hydrate formation. THF crystallization and its subsequent melting were detectable during cooling to 133 K.

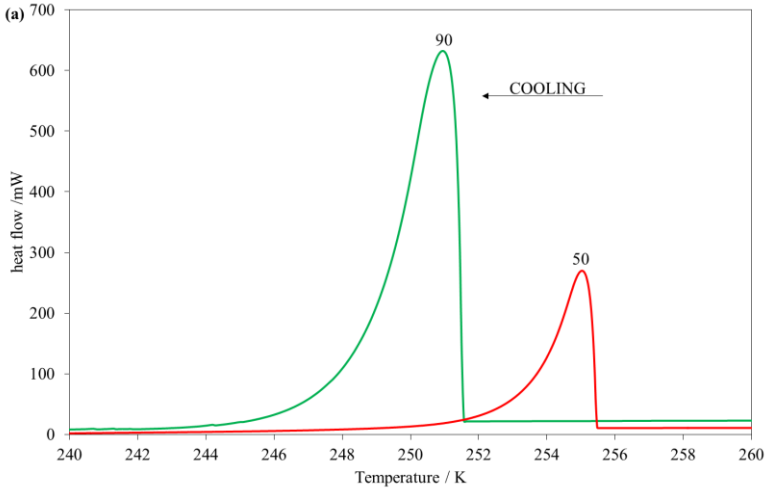
(a)
90
COOLING
50
heat flow /mW
Temperature / K

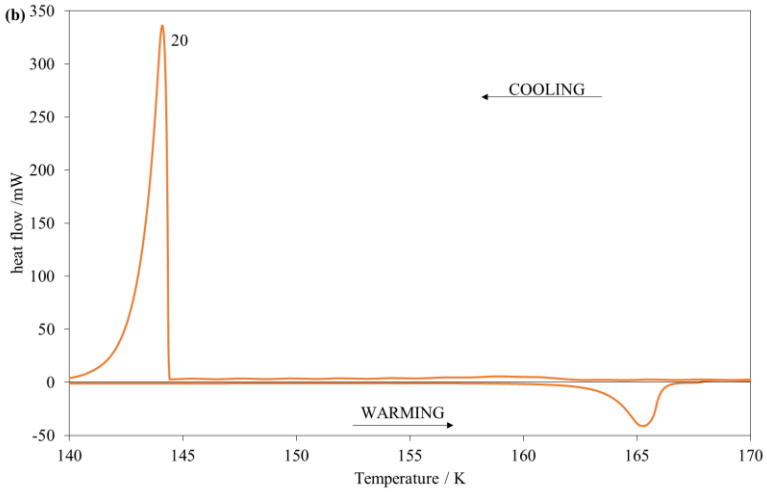
(b)
20
COOLING
WARMING
heat flow /mW
Temperature / K

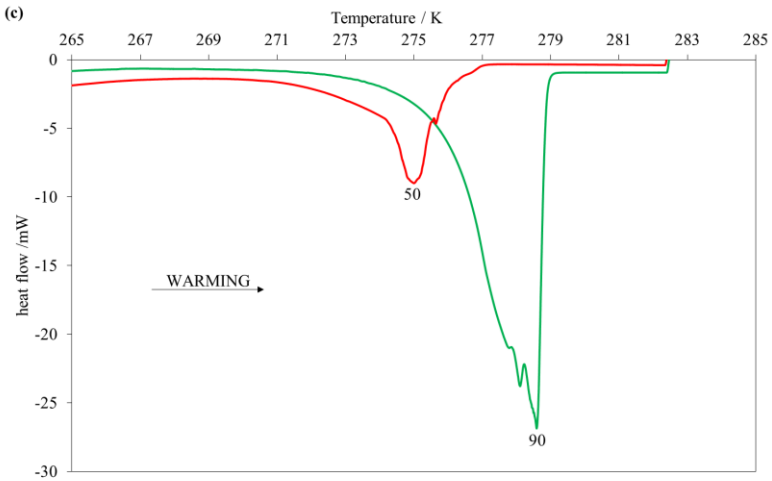
(c)
Temperature / K
50
WARMING
90
heat flow /mW

Figure 5. Typical thermograms of crystallization and melting of THF-rich samples: (a) hydrate crystallization during cooling, (b) THF crystallization and melting and (c) hydrate melting.

For samples using THF excess, hydrate formation and dissociation were detected up to a THF concentration of 82.6 Wt% in the initial THF-H_2O mixture (Fig.5a and c). No evidence for ice crystallization or melting has been found in any THF oversaturated samples. At low temperatures, the crystallization and melting of THF could be observed (Fig. 5b).

3.1.2. Variations in onset and offset temperatures of ice and hydrate melting

Due to the above described variation during phase crystallization, further investigations focus only on melting events of ice and THF hydrate. The onset and offset temperatures of melting events are graphical constructions and defined as the intersection of the tangents of the peak flanks with the baseline.

The equilibrium temperature of THF hydrate depends on the fraction of THF in the initial solution. Generally, the here observed onset temperatures of THF hydrate formed from both, H_2O- or THF-rich solutions are broadly in agreement with literature values reported for THF–H_2O phase changes (Fig. 6 and references therein). The onset temperature is highest at expected hydrate saturations of 100 Vol% which corresponds to the THF content of 19 Wt% in the initial solution. The maximum value of 276.9 K detected here, is slightly below values reported in the literature which are between 277.4 K and 278 K [2,20,22]. With decreasing hydrate content and hence increasing content of an excess phase of either H_2O or THF, the onset temperatures of THF hydrate melting decrease. In this study, lowest values have been detected with 274.8 K for a H_2O-rich solution with 6.7 Wt% THF in the initial solution which corresponds to an expected

hydrate concentration of 36.2 Vol%. For the THF-rich solution with 82.6 Wt% THF in the initial sample, corresponding to an expected hydrate content of 20.1 Vol%, an onset temperature of THF hydrate melting of 266.7 K has been determined. This is in agreement with published data of Jones et al. [31]. The detected onset temperatures of H_2O-rich samples have a rather linear trend and show slightly lower values compared to literature data. This might be caused by the differences in methods of preparation and determination of the start of hydrate melting temperature.

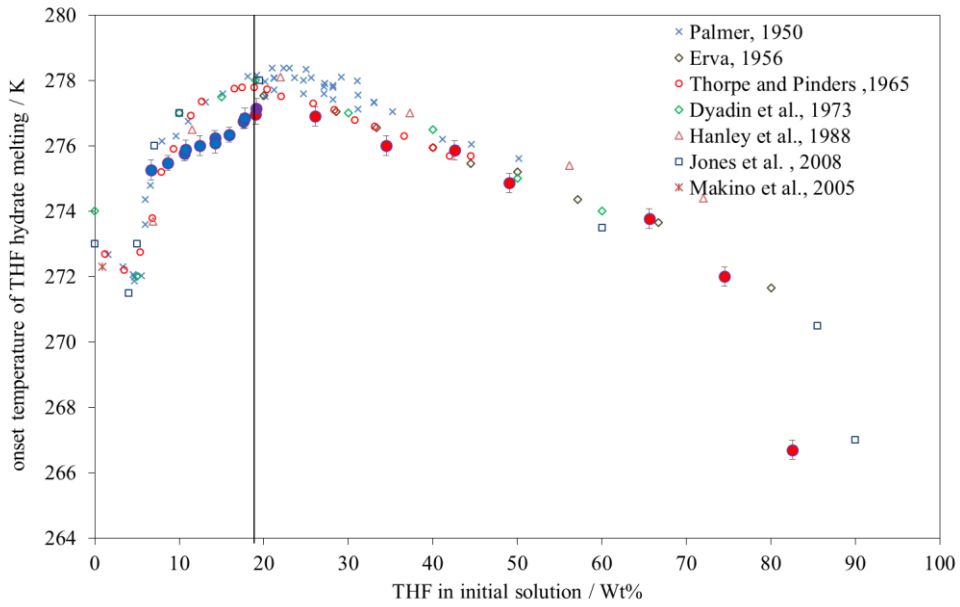

Figure 6. THF hydrate onset temperatures at ambient pressure of this study in comparison to melting temperatures from the literature. Blue dots show the onset temperature of hydrate melting formed from a H_2O-rich solution, red dots show the onset temperature of hydrate melting from THF-rich samples. All other marks are taken from literature (see legend for references) [14,22,23,24,29,30,31].

The onset and offset temperatures of ice melting of pure H_2O measured in this study are with 273.4 K and 274.4 K, respectively, in agreement with literature data [13]. We observed that the onset temperatures of ice melting slightly decrease with increasing THF content in the initial

solution from 272 K for a 2.3 Wt% THF solution to 271.7 for a 19 Wt% THF solution (Fig. 7). The offset temperatures show a more pronounced decrease with increasing THF content. While a 2.3 Wt% THF solution results in an ice offset temperature of 273.5 K, at 17.6 Wt% THF in solution the offset temperature decreased to 272.5 K. This is caused by the decreasing amount of free/excess H_2O with increasing content of THF in the initial solution. This leads to a reduced peak area for the enthalpy of ice melting not only in its amplitude but also in its range (see Fig. 4).

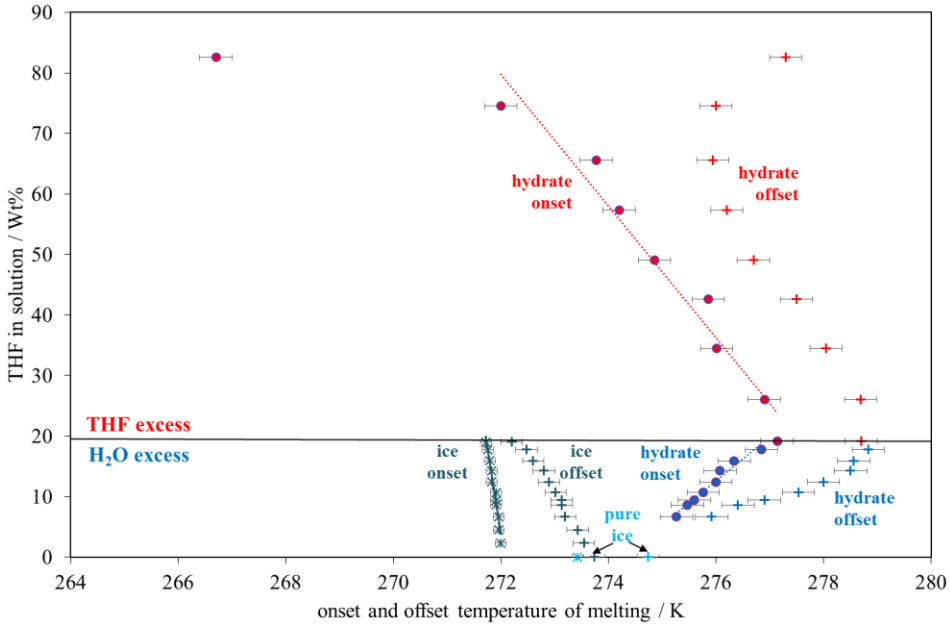

Figure 7. Onset and offset temperatures of ice and THF hydrate melting in dependence on the THF concentration of the initial solution.

The on- and offset temperatures of THF hydrate melting in the H_2O-rich system show the opposite trend. Both temperatures increase with increasing THF content in the initial solution. The onset temperatures of THF hydrate dissociation vary between 275.3 K and 276.9 K and the offset temperatures range between 275.8 and 278.7 K for THF concentrations of 6.7 and

19.1 Wt% in the initial solution, respectively. We observed that the higher the THF hydrate content, the larger is the distance between onset and offset temperature of hydrate melting. This fact is owed to the increasing hydrate amount in the sample resulting in an increasing peak area. The lower the THF content in the initial sample, the more converges the THF hydrate melting peak towards lower temperature and hence into the ice melting peak. At low THF concentrations (6.7 Wt%) in the initial solution, the endotherms of ice and hydrate melting merge. For this reason, THF hydrate was not detectable in samples with less than 6.7 Wt% THF in the initial solution due to the overlay of the small hydrate melting endotherm by the large endotherm of ice melting. In addition, composition and temperature are close to eutectic conditions supporting the assumption of a certain overlap of ice and hydrate melting events. Based on Raman spectroscopic investigations shown below, at concentrations of 5 Wt% THF in the initial solution first hydrate was found (at 273,65 K). This in turn may lead to the assumption that either the content of hydrate is very low or no hydrate occurs at these low initial THF concentrations.

The onset and offset temperatures of THF hydrate melting decrease with an increasing excess of THF in the initial solution. This follows a fairly linear trend up to 75 Wt% THF in solution. A higher THF excess, attended by an even lower THF hydrate content in the sample causes a strong deviation from this trend. Here, hydrate melting results in an endotherm that is shallow and wide in appearance. The early start of THF hydrate dissociation and the high offset temperature suggest that there might be several metastable hydrate phases present that melt one after the other.

For some THF-rich samples, cooling to 133 K was performed to induce freezing of the excess THF and to determine the melting conditions during subsequent heating. The on- and offset temperatures of THF melting show only small variations with changing THF concentrations

which can be attributed to the growing peak size with increasing THF content in the sample. The detected onset temperature of pure THF melting is 163.4 K. This is below literature data which state values between 164.05 K and 165.1 K [e.g. 32,33] and can be caused by extrapolation deviations at low temperatures.

Due to the linear trend of onset temperatures of ice and hydrate melting in H_2O- or THF-rich solutions (see trend curves in Fig. 7), the melting point depression might be used to calculate the THF content of the initial solution using one of the following best fit equations.

$$THF / Wt\% = -63.072 \times T_{ice\ melting}\ (\pm 0.1)/\ K + 17159 \qquad (R^2 = 0.9533) \qquad (1)$$

$$THF / Wt\% = 7.1058 \times T_{hydrate\ melting}\ (\pm 0.3)/\ K - 1948.9 \qquad (R^2 = 0.9715) \qquad (2)$$

$$THF / Wt\% = -10.721 \times T_{hydrate\ melting}\ (\pm 0.3)/\ K + 2995.2 \qquad (R^2 = 0.9442) \qquad (3)$$

The calculations might be helpful in testing the correctness of solutions or to determine the composition of unknown THF-H_2O solutions.

Generally, on- and offset temperature of hydrate melting decrease with deviation from the stoichiometric THF:H_2O ratio in the initial solution. The melting point depression can be explained by a stronger disequilibrium in highly H_2O or THF deficient systems. Similarly, with increasing content of H_2O in the sample, the ice stability increases, which is indicated by increasing onset and offset temperatures: the highest on- and offset temperatures of ice were detected at low THF concentration in the initial solution.

Secondly, the higher the content of the ice or the hydrate phase the larger the related area of endotherm of melting. This is mirrored by expanding distances between onset and offset temperature of the melting events in the case of H_2O-rich samples. Interestingly, it does not

apply to the THF-rich system. Here, peak width increases with lower hydrate content and the amplitude of the peak decreases. This suggests incongruent melting of more than one hydrate phase within a larger temperature range. THF-rich fluid inclusions within the hydrate might also influence the melting pattern.

3.1.3. Variations of specific enthalpy of THF, ice and THF hydrate melting

The peak area represents the amount of heat that is consumed by the sample during transition and is proportional to the total enthalpy of melting. The specific enthalpies (J/g) of melting events were calculated by integration of the peak areas divided by the expected sample mass of THF, ice and hydrate, respectively. The expectations refer to the theoretically complete conversion of THF and H_2O into hydrate with full cage occupancy and one pure excess component remaining.

For instance, a H_2O-rich sample that contains 90.6 Wt% H_2O and 9.4 Wt% THF should, upon cooling, form 50 Vol% THF hydrate and 50 Vol% ice from the excess pure H_2O phase. Assuming this complete reaction, ice and THF hydrate would melt during subsequent warming and produce two endotherms with peak areas of half the area of a pure ice or pure THF hydrate.

For pure ice, the measured enthalpy of melting of 343 J/g is in agreement with literature values (e.g. 336 +/- 3 J/g) [13]. For a completely converted sample with 50 Vol% (50.7 Wt%) ice, the endotherm of ice melting should consequently cover an area that equals 164.7 J/g. However, measured values are higher, in this case the enthalpy of ice melting is 191.8 J/g. Generally, for ice melting the measured enthalpies exceed the theoretically expected data by 10.8 to 55.8 J/g, which in turn corresponds to 3.2 to 16.7 Wt% H_2O that is overly in excess than expected.

The stoichiometric THF-H_2O mixture of 19.1 Wt% THF and 80.9 Wt% H_2O should result in a pure THF hydrate with melting enthalpies similar to literature values of 262.9 J/g or 260 J/g [12,13]. But enthalpy of melting of THF hydrate is with 248.9 J/g somewhat lower. When assuming complete reaction, there should be no excess of both, THF or H_2O. Nevertheless, we observed one endotherm that indicates ice melting besides the THF hydrate melting endotherm. In contrast, the crystallization or melting of a THF phase could not been observed upon freezing to 133 K. This can be caused by the incorporation of more THF into the hydrate than commonly assumed. THF might also remain as minor component in the excess aqueous phase. The melting point depression of ice would support the latter.

In fact, THF crystallization and melting was only observed in samples with THF in excess. Here the deviation of expected and actual enthalpy of THF melting is small (Fig 8). All measured enthalpy values are slightly below the expected values, which means that less THF is present in the excess phase than expected. The “missing” volume of THF is, based on the difference of expected and measured enthalpy values between 1.3 and 3.9 J/g, between 1.1 and 3.4 Wt% THF. Based on microscopic observations on hydrates formed from THF excess solutions, it is likely to be present in form of fluid inclusions within hydrate. No H_2O -related melting or crystallization events were observed in THF-rich samples.

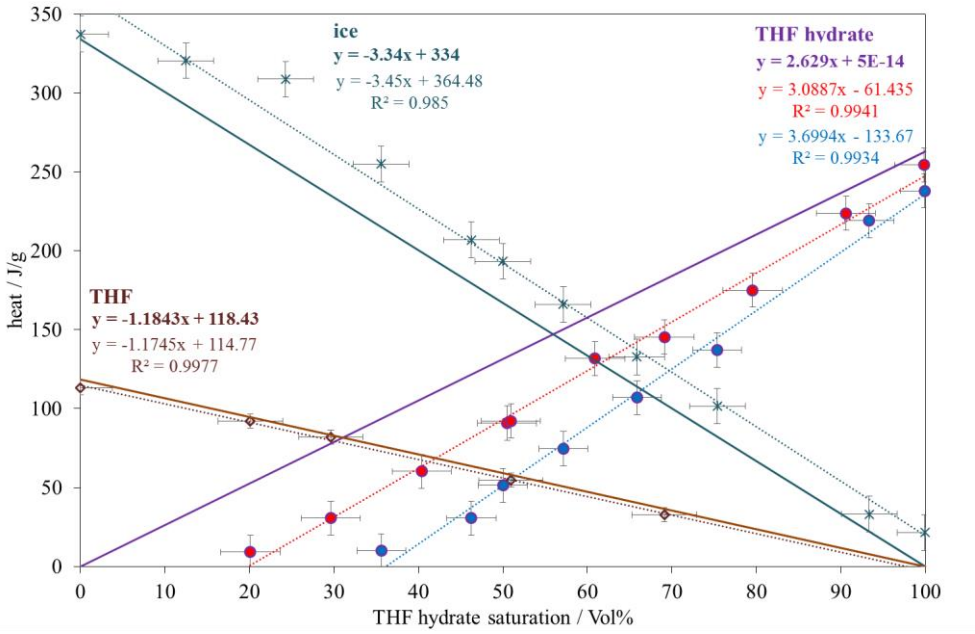

Figure 8. Deviation of heat values from theoretically expected hydrate saturations for complete conversion. The measured data of ice melting (stars), THF melting (open diamonds), hydrate melting in H_2O excess (blue dots) and hydrate melting in THF excess (red dots) are shown in comparison to theoretical expectations (blue, brown and violet lines for ice melting, THF melting and hydrate melting, respectively). In addition, best fit equations for complete conversion and for measured data are shown. The uncertainties of enthalpy values are stated in Table Table 3. Experimental results of calorimetric measurements. and are based on repeated measurements, the uncertainties of THF hydrate saturation result from calculations using the best fit equations.

The enthalpy of hydrate melting of both, formed from THF- or H_2O -rich initial solutions, deviate negatively from the ideal calculation. For a sample that theoretically results in a 50 Vol% (49.3 Wt%) hydrate saturation and 50 Vol% excess, the peak area of the respective THF hydrate melting ideally results in an enthalpy of 129.6 J/g. The measured value of melt enthalpy is, however, considerably lower with only 51.3 J/g in H_2O-rich samples and 90.8 J/g in THF-rich samples. The deviations increase with decreasing expectations on hydrate content. For H_2O -rich samples, the expected hydrate fraction of 30 Vol% is in fact only 5 Vol%. For THF excess with 82.7 Wt% in the initial solution 5 Vol% hydrate instead of expected 20 Vol% are formed.

Generally, the results show that hydrates formed from H_2O-rich solutions show much lower enthalpy values which means that the hydrate formation is much less complete than estimated by calculations for full conversion. The enthalpy of hydrates formed from H_2O -rich solution is between 64 and 93 J/g below expectations. The values measured for hydrates formed from THF-rich solutions deviate also negatively but only between 24 and 50 J/g. For the stoichiometric solution containing 19.1 Wt% THF in the initial solution, the hydrate deficiency is lowest with 4 Vol%.

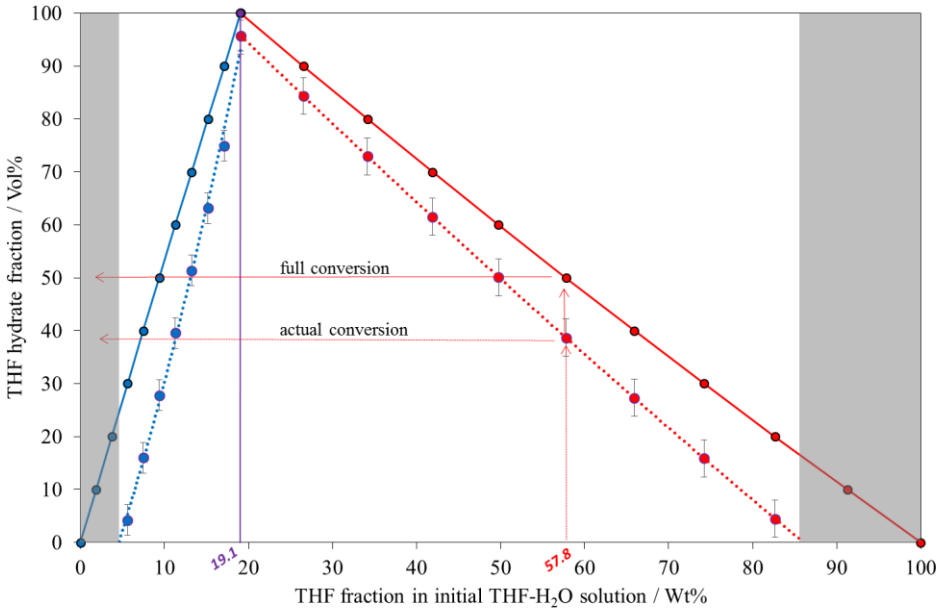

Figure 9. Comparison of theoretical calculations (see Fig. 1) assuming full conversion of THF and H_2O (bold line) and calculated values based on the measurements of enthalpy of melting of hydrate (stippled line). Blue color indicates H_2O excess, red indicates THF excess in the initial solutions.

It is not possible to proclaim a percentage for correcting the initial solution. We used the best fit equation of the measured enthalpy values (Fig. 8) for the calculation of the amount of hydrate that is dissociated. By plotting these values versus the initial THF fraction in solution (Fig. 9),

two polynomial equations describe the actual relationship between THF in solution and THF hydrate fraction with a coefficient of determination of 0.9965 and 1 for H_2O-rich and THF-rich solutions, respectively.

$$\text{Hydrate / Vol\%} = 0.0929 \times [\text{THF}_{\text{initial}} / \text{Wt\%}]^2 + 4.2366 \times [\text{THF}_{\text{initial}} / \text{Wt\%}] - 21.3323 \quad (4)$$

$$\text{Hydrate / Vol\%} = 0.0016 \times [\text{THF}_{\text{initial}} / \text{Wt\%}]^2 - 1.5927 \times [\text{THF}_{\text{initial}} / \text{Wt\%}] + 125.51 \quad (5)$$

For instance, an initial solution containing 57.8 Wt% THF the formed hydrate fraction is not, as expected 50 Vol%, but in fact only 38.8 Vol%.

Table 4. Expected hydrate saturation (calculated based on Tab. 1) in comparison to hydrate saturation calculated using correction equation (4) and (5) in dependence of initial THF:H_2O ratio. Blue marks H_2O-rich initial solutions, red marks THF-rich initial solutions and violet marks the stoichiometric solution. The uncertainties of the achieved hydrate saturation are based on calculations using best fit equations of Fig. 8 and the uncertainties of enthalpy measurements as stated in Table 3. Experimental results of calorimetric measurements.

H_2O in initial solution	THF in initial solution	**expected hydrate saturation**	expected excess H_2O/THF	**achieved hydrate saturation**	calculated uncertanties
Wt%	Wt%	**Vol%**	Vol%	**Vol%**	Vol%
98.1	1.9	**10**	90		
96.3	3.7	**20**	80		
94.4	5.6	**30**	70	**5.3**	± 2.9
92.5	7.5	**40**	60	**15.6**	± 2.9
90.6	9.4	**50**	50	**26.7**	± 2.9
88.7	11.3	**60**	40	**38.4**	± 2.9
86.8	13.2	**70**	30	**50.9**	± 2.9
84.8	15.2	**80**	20	**64.2**	± 2.9
82.9	17.1	**90**	10	**78.3**	± 2.9
80.9	19.1	**100**	0	**95.7**	± 3.5
73.5	26.5	**90**	10	**84.4**	± 3.5
65.9	34.1	**80**	20	**73.0**	± 3.5
58.1	41.9	**70**	30	**61.6**	± 3.5
50.2	49.8	**60**	40	**50.2**	± 3.5
42.2	57.8	**50**	50	**38.8**	± 3.5

34.1	65.9	**40**	60	**27.5**	± 3.5
25.8	74.2	**30**	70	**16.1**	± 3.5
17.3	82.7	**20**	80	**4.8**	± 3.5
8.8	91.2	**10**	90		

The composition of the excess liquid phase cannot be to determine by calorimetry. For H_2O - rich samples and samples with stoichiometric composition only an ice melting event has been observed next to hydrate melting but no THF crystallization or melting could be detected. Vice versa, for THF-rich samples only the THF crystallization and melting was observable but no ice crystallization or melting. Nevertheless, we assume that the corresponding minor phase is present, but, due to its low concentration and the full miscibility, assimilates to the dominant excess phase. An indication for this behavior is the melting point depression of the ice formed from excess H_2O.

These findings are indicative for the commonly known incomplete conversion of THF and H_2O into hydrate and the aim for chemical equilibrium between the three components THF, H_2O and THF hydrate. However, even though the fact of the incomplete conversion of THF and H_2O into hydrate is recognized, so far there is no measure known to the authors to correct the initial solution to form a defined hydrate-excess ratio in the final sample volume. Based on the data obtained here, we conclude that hydrate contents in experimental simulations might largely be overestimated and correction is necessary, especially for lower hydrate contents and for experiments using H_2O as the excess phase.

Incomplete cage occupancy is likely to occur in the H_2O-rich system and with increasing H_2O excess in the sample this effect might become even more pronounced. This would explain the stronger deviance of enthalpy values of the THF-H_2O samples with H_2O in excess compared to

the THF-rich samples. For the latter, the cage occupancy can be assumed to be complete due to the surplus of guest molecules.

The presence of air hydrate alongside THF hydrate formation cannot be confirmed. According to Gough and Davidson and references therein, the occurrence of air hydrate results in higher stability and higher melting temperatures [19,22,34,3]. Both were not observed in our investigations.

3.2. Raman spectroscopic measurements

The calibration measurements of the Raman spectra taken from the initial THF-H_2O mixtures show a definite correlation between THF concentration and integrated intensity of the Raman signal (Fig. 10) as well as a very good reproducibility. The Raman spectra presented in Figure 9 show characteristic Raman bands of THF: the small band at 890 cm^{-1} can be assigned to the COC+CH_2 mode whereas the larger band at 920 cm^{-1} can be assigned to the C-C-C-C stretching mode [9]. It should be noted that Raman spectra of THF in THF-H_2O mixtures differ significantly from a Raman spectrum of pure THF. For pure THF the C-C-C-C stretching modes and the COC+CH_2 modes can be observed as a major band at 915 cm^{-1} [35,16]. For the THF-H_2O mixture, the C-C-C-C and the COC+CH_2 modes are clearly separated bands. Takasu et al. assume that hydrogen-bond formation between a THF molecule and H_2O molecules alter the position of the C-C-C-C stretching mode to higher energy side and that of the COC+CH_2 mode to lower energy side [16]. In our Raman spectroscopic measurements we observed a shift of the band at 1029 cm^{-1} (pure THF) to 1037 cm^{-1} when THF is dissolved in H_2O. This band can be assigned to several modes such as CH_2-wagging, CH_2-twisting, CH_2-rocking, C-C stretching and COC stretching [18].

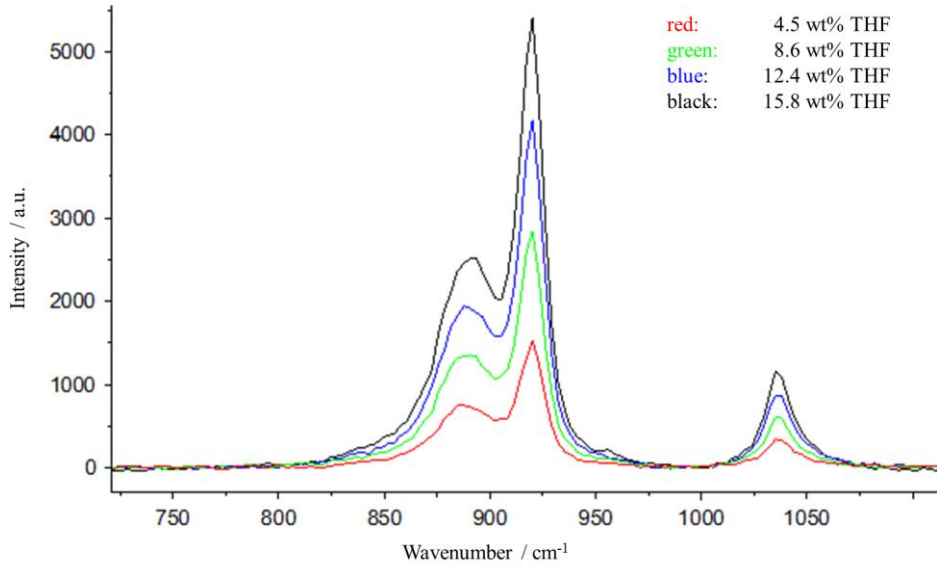

Figure 10. Raman spectra of THF-H_2O mixtures (initial solution, H_2O excess). The spectra clearly show the correlation between increasing THF concentration in solution and increasing Raman intensity.

For the generation of a calibration graph we choose the band at 1037 cm^{-1} because it is clearly separated from other bands. The evaluation of the integrated intensities shows a good reproducibility with low deviations (<5%). The calibration graph in Figure 11 shows the correlation between the integrated intensities (a.u.) and the mass percentage [Wt%] of THF in the THF-H_2O initial solution.

As mentioned in the experimental methods part, the initial THF-H_2O mixtures were frozen in a freezer at 263 K until a solid phase (hydrate/ice) formed. Thereafter, the samples were placed in a cooling box and carefully warmed to 273.65 K or 275.15 K until the ice phase melted and the hydrate phase besides a coexisting aqueous phase remained. Depending on the volume of the coexisting aqueous phase, 2-3 samples were taken from the coexisting aqueous phase and analyzed via Raman spectroscopy.

At 273.65 K, THF-H_2O mixtures containing less than 5 Wt% THF in the initial solution did not show a hydrate phase present. This observation is in agreement with data from Erva showing that at this temperature no THF hydrate forms from solutions containing less THF [23]. The Raman spectra taken from these mixtures were similar to those of the initial solution. In samples formed from THF-H_2O mixtures containing more than 5 Wt% (X_{THF}= 0.013) THF in the initial solution a hydrate phase is present. For samples taken from the excess aqueous phase the integrated intensities of the Raman bands at 1037 cm^{-1} show similar values compared to those obtained from the THF-H_2O mixtures containing 5 Wt% THF. This was observed for all excess aqueous phases containing coexisting hydrate regardless of the composition of the initial solution.

At slightly higher temperatures of 275.15 K, a hydrate phase was observed first in samples containing more than 6.6 Wt% THF in the initial solution. No hydrate phase could be detected in samples of lower THF concentrations. This in fact indicates that hydrates in samples of 5 Wt% THF in initial solution already dissociate before 275.15 K, even though this is still below the actual melting point of THF hydrate of 277.4 K. This is again in good agreement with literature data [23] as well as with findings from calorimetric measurements that show the shift in onset melting temperatures of THF hydrate towards lower values with decreasing THF content in the initial solution. For the coexisting aqueous phase besides a hydrate phase the integrated intensities of the Raman bands at 1037 cm^{-1} show almost the same values compared to those obtained from the THF-H_2O initial solution containing about 7 Wt% THF (X_{THF}=0.018).

Figure 11 shows the measured integrated intensities of the Raman band at 1037 cm^{-1} of Raman spectra taken from the coexisting aqueous phases besides the hydrate phase formed from

different THF-H_2O initial solutions. The percentage by mass of THF in the initial THF-H_2O solution is given in the abscissa.

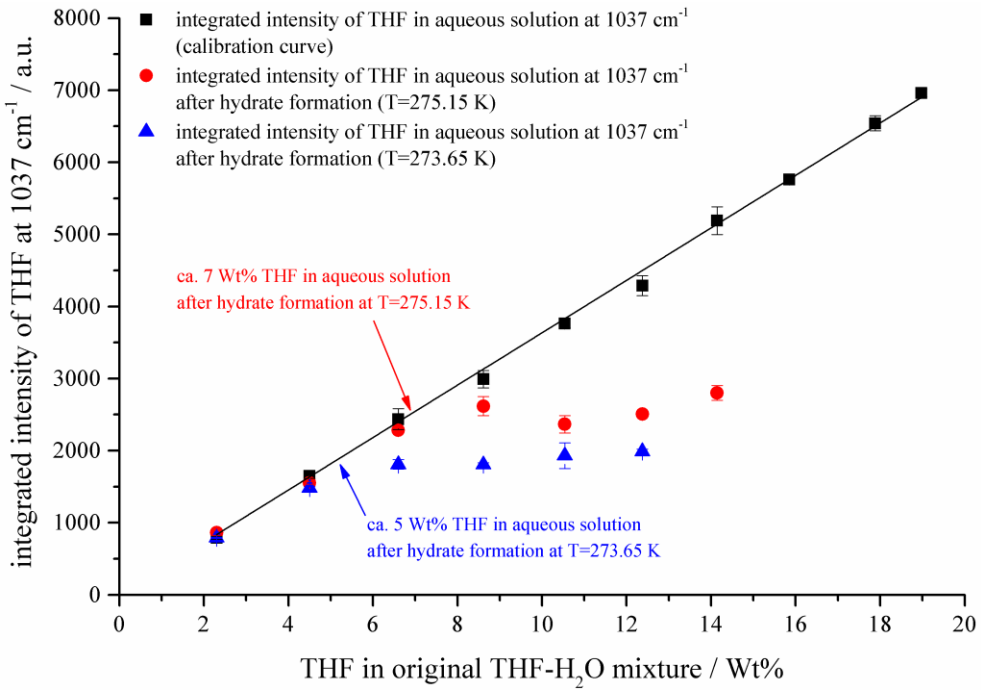

Figure 11. Determination of the percentage of THF by mass in the coexisting aqueous phase via integrated intensities of the Raman bands at 1037cm^{-1}.

For the determination of the composition of the hydrate phase, 2-3 hydrate crystals formed from the initial solutions (H_2O excess, T=273.65 K) were transferred into a Linkam cooling stage. At least 3 spectra were taken at different areas of the crystal. The Raman spectrum of THF in a hydrate phase differs significantly from the Raman spectrum of THF dissolved in the H_2O phase. Similar to pure THF the C-C-C-C stretching modes and the COC+CH_2 modes can be observed as a major band at about 915 cm^{-1}. Based on the integrated intensities of the Raman bands at 915 cm^{-1} (THF) and the broad band 3050 - 3600 cm^{-1} (H_2O) we calculated the ratio of THF to H_2O in the hydrate crystals. The results are shown in Figure 12. The results show broad

variations of the THF:H_2O ratios in the hydrates and no correlation with the composition of the initial solutions. The scattering of the hydrate compositions indicates that hydrates are not in equilibrium and did not reach the stoichiometric composition consistently.

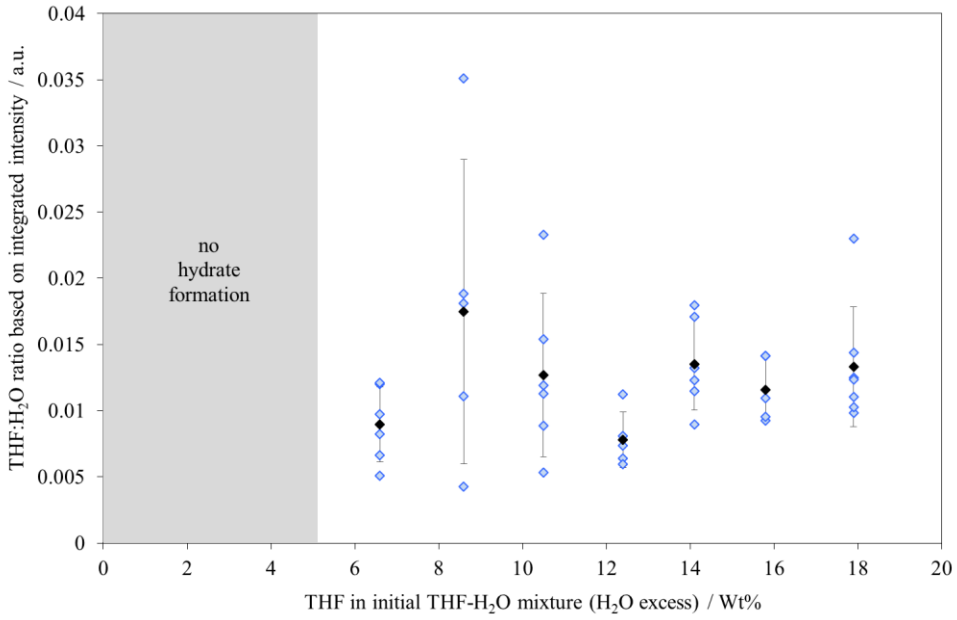

Figure 12. THF:H_2O ratios in hydrate crystals formed from THF-H_2O initial solutions with H_2O excess. The THF:H_2O ratio was calculated from the integrated intensities of the Raman bands at 915 cm^{-1} and 3050-3600 cm^{-1}. The blue diamonds refer to the single measurements. The black diamonds represent the mean values including error bars resulting from the standard deviation.

Similar experiments were performed with THF-H_2O mixtures with THF in excess. Unfortunately, we were not able to obtain reproducible Raman spectra from the samples with constant composition with respect to the integrated intensities. Therefore, we were neither able to calculate a calibration curve nor to quantify the H_2O content in the coexisting THF-rich liquid phase besides the hydrate phase. However, the Raman spectra do indicate that some H_2O remains in the coexisting THF-rich liquid phase and is not transformed into hydrate. This was observed

for all THF-H_2O mixtures with THF excess. At concentrations <9.2 Wt% H_2O (>90.8 Wt% THF) in the initial solution no hydrate formation could be observed. For all other mixtures we were able to analyze the hydrate phase. Figure 13 shows the THF:H_2O ratio of the resulting hydrate phases formed from different THF-H_2O mixtures and based on the integrated intensities of the Raman band at 915 cm^{-1} (THF) and at 3050-3600 cm^{-1} (H_2O).

The results show a strong variation of the THF:H_2O ratio in the hydrate phase, which again indicates that the hydrate does not reach a homogenous, stoichiometric composition as expected for the equilibrium state. Furthermore, in some of the analyzed hydrate crystals fluid inclusions were observable. This may also explain the strong variation of the THF:H_2O ratio and the overall higher values for the THF-H_2O ratio in the hydrate crystals formed from a THF-H_2O mixture with THF excess compared to those hydrate crystals formed from a THF-H_2O mixture with H_2O in excess.

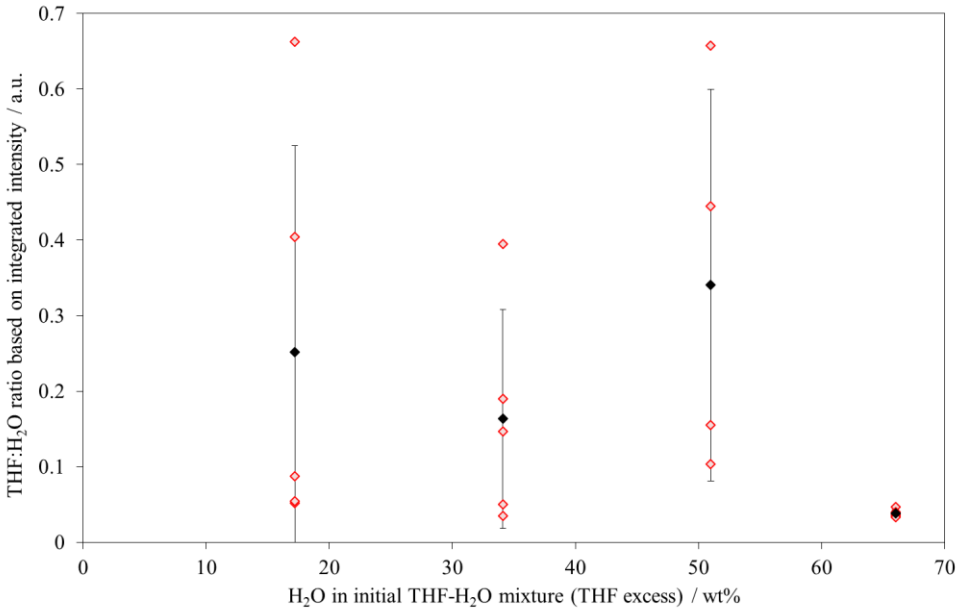

Figure 13. THF:H_2O ratios in hydrate crystals formed from initial solutions with THF excess. The THF:H_2O ratio was calculated from the integrated intensities of the Raman bands at 915

cm^{-1} and 3050-3600 cm^{-1}, respectively. The blue diamonds refer to the single measurements. The black diamonds represent the mean values including error bars resulting from the standard deviation.

4. SUMMARY AND CONCLUSIONS

In this study we investigated the phase behavior of THF-H_2O mixtures with excess H_2O or THF at ambient pressure, with the foremost aim to determine the ability of THF hydrate as a substitute for methane hydrate in laboratory studies.

In the course of preparation, a considerable length of undercooling of the THF-H_2O solution to about 250 K is recommended to assure hydrate formation. Calorimetric results visualize the formation of hydrate and ice subsequent to supercooling by the occurrence of one or two exotherms at temperatures between 270 K and 245 K. whereby first hydrate crystallizes and secondly ice. In a large number of measurements, independent of the THF:H_2O ratio, a simultaneous formation of both ice and hydrate occurs.

The onset temperature of hydrate melting is in agreement with literature values. Both, onset and offset temperatures of hydrate melting increase towards stoichiometric composition of the initial solution which is 19.1 Wt% THF and 80.9 Wt% H_2O. The on- and offset temperatures of ice formed from the excess H_2O phase decrease with increasing hydrate content. Temperatures of ice and hydrate melting can be used to calculate the initial THF concentration and vice versa.

In H_2O-rich samples, the endotherms of ice and hydrate melting are distinct when high hydrate saturations are expected. However, the lower the expected hydrate saturation, the stronger merge the two endotherms. Below an expected hydrate saturation of 35 Vol% (6.7 Wt% in initial solution) the hydrate-related endotherm disappears, either by being overlapped by the even

further growing ice melting endotherm or by eventually overstepping the eutectic composition towards the ice-liquid stability field where no hydrate is present.

The observations are in agreement with Raman spectroscopic measurements on H_2O-rich samples. At 273.65 K, hydrate did not occur below 5 Wt% THF in the initial solutions. Measurements at 275.15 K show first hydrates from a 7 Wt% THF solution. These values are in agreement with literature data determined at equilibrated samples. However, the investigated hydrate samples show very heterogeneous composition indicating that the hydrate phase did not reach equilibrium state.

For hydrate formed from THF in excess the lowest hydrate concentrations detected was 20 Vol%, corresponding to 82.7 Wt% THF in the initial solution. Raman analyses identify evidence for H_2O remains in the coexisting THF-rich liquid phase at all concentrations which is indicative for an incomplete transformation of H_2O into hydrate.

The measured values of specific enthalpy for ice and THF hydrate melting in THF-H_2O mixtures deviate strongly from expectations. While the specific enthalpies of ice melting are above expected data, the specific enthalpies of THF hydrate are considerably below expected values. This indicates an unfinished conversion of THF and H_2O into hydrate. Based on calorimetric data the amounts of hydrate formed from H_2O-rich samples are between 4.3 and 25 Vol% below expectations, for THF-rich samples the deviations are 4.3 to 15 Vol% less than expected. The deviation of 4.3 Vol% applies to the stoichiometric solution that should theoretically result in a full conversion with no excess THF or H_2O. The deviations from expectations increase with increasing excess phase. Two equations are proposed to correct for the deficiency in final hydrate volumes.

Especially if geophysical measurements rely on an exact determination of the amount of the hydrate phase, THF hydrate is not a straightforward substitute. This is particular true for applications were low hydrate saturations are needed. The use of THF hydrate as a substitute for CH_4 hydrate can therefore only be recommended for intermediate to high hydrate saturations and when corrections to the initial THF-H_2O solution are made. The common calculations based on stoichiometric measures do not result in correct hydrate saturations.

With the approach to create a stable and well-defined liquid-hydrate sample, applicable to mimic hydrate-bearing sediments, THF-excess is more reliable. Even though, H_2O is the actual liquid phase in nature - paired with THF and ambient pressure, only a very narrow temperature range (after ice melting, before hydrate dissociation) can be used for experiments in which two phase H_2O-THF hydrate system is present. At low hydrate contents, the hydrate dissociation will already initiate at these temperatures and below eutectic concentrations no hydrate is present at all.

By choosing THF as the excess liquid phase, the applicable working temperature extends towards lower values where THF hydrate finds itself in a reliably stable state within the two phase liquid-solid system. However, microscopic and Raman spectroscopic measurements indicate the incorporation of liquid THF as fluid inclusions into the solid hydrate phase. This may also influence the geomechanical properties of the THF hydrate phase. Also, because THF is a highly volatile substance, the experiments should be performed in a closed system to avoid permanent changes of the equilibrium and hence hydrate composition in the course of an experiment.

REFERENCES

[1] Morrison, R.T., Boyd R.N., *Lehrbuch der Organischen Chemie* 3rd Edition, 1986, VCH, Weinheim.

[2] Sloan, E.D., Koh, C.A., *Clathrate Hydrates of Natural Gases*. 3rd ed.; CRC Press: Boca Raton, FL, 2008; p. 72.

[3] v. Stackelberg, M., Meinhold, W., Zeitschrift für Elektrochemie 1954, 40-45.

[4] Lee, J.Y., Yun, T.S., Santamarina, J.C., Ruppel, C.A., *Geochem. Geophys. Geosys.* 2007, 8, Q06003, doi:10.1029/2006GC001531.

[5] Rueff, R.M., Sloan, E.D., *Ind. Eng. Chem. Proc. Des. Dev.* 1985, *24*, 882-885.

[6] Pearson, C., Murphy, J., Hermes, R.J., *Geophys. Res.: Solid Earth* 1986, *91*, 14132-14138.

[7] Yun, T.S., Francisca, F.M., Santamarina, J.C., Ruppel, C.A., *Geophys. Res. Lett.* 2005, *32*, DOI: 10.1029/2005gl022607.

[8] Yun, T.S., Santamarina, J.C., Ruppel, C.A., *J. Geophys. Res.: Solid Earth* 2007, 112, DOI: 10.1029/2006JB004484.

[9] Rydzy, M.B., *PhD Thesis*, 2014, Colorado School of Mines, 2014.

[10] Priegnitz, M. *Master Thesis*, 2012. Christian-Albrechts-Universität zu Kiel, 2012.

[11] Rosso, J.C., Carbonnel, L., *C.R. Acad.Sc.*, 1971, t. 273, Serie C, 15-18.

[12] Leaist, D.G., Murray, J.J., Post, M.L., Davidson, D.W., *J. Phys. Chem.* 1982, *86*, 4175-4178.

[13] Handa, Y.P., Hawkins, R.E., Murray, J.J., *J. Chem. Thermodyn.* 1984, *16*, 623-632.

[14] Makino, T., Sugahara, T., Ohgaki, K., *J. Chem. Eng. Data* 2005, *50*, 2058-2060.

[15] Bondarev, E., Groisman, A., Savvin, A., *Proceedings of the 2nd International Conference on Natural Gas Hydrates*; Toulouse, France, June 2-6, 1996.

[16] Takasu, Y., Matsumoto, S., Fujii, Y., Nishio, I., *Chem. Phys. Lett.* 2015, *627*, 39-43.

[17] Alavi, S., Susilo, R., Ripmeester, J.A., *J. Chem. Phys.* 2009, *130*, 174501.

[18] Von Stackelberg, M., Meuthen, B., *Z. Electrochem*.1958, 62-130.

[19] Gough, S.R., Davidson, D.W., *Can. J. Chem*. 1971, 49, 2691,

[20] Dervakonda, S., Groysman, A., Myerson, A.S., *J. Cryst. Growth*. 1999, 204, 525-538.

[21] Ganji, H., Manteghian, M., Sadaghiani Zadeh, K., *J. Chem. Eng. Jp,* 2006, Vol. 39, 4, 401-408.

[22] Palmer, H.A., *PhD thesis*, University of Oklahoma, 1950

[23] Erva, J., *Suomen kemistil.* 1956, *29B*, 186.

[24] Thorpe, B.D., Pinders, K.L., *Suomen Kemist.* 1965, J. 38B**.**

[25] Riddick, J., *Organic Solvents Physical Properties and Methods of Purification. Techniques of Chemistry*. 1970. Wiley-Interscience. Table of Physical Properties, Water 0b.

[26] O'Neil, M.J. *The Merck Index. An Encyclopaedia of Chemicals, Drugs and Biologicals*. 2013, 15th Edition Edited by M.J. O'Neil, Royal Society of Chemistry, Cambridge, UK.

27 Rydzy M.B., Schicks J.M., Naumann R., Erzinger J., *J Phys Chem B.*, 2007 16, 111(32):9539-45.

[28] Tombari, E., Presto, S., Savetti, G., Johari, G.P., *J. Chem. Phys*. 2006, 124, doi: http://dx.doi.org/10.1063/1.2188944.

[29] Dyadin, Y.A., Kuznetsow, P.N., Yakovlev, I.I., Pyrinova, A.V. *Dokl. Akad. Nauk SSSR*, 1973, V 208, 1, 103-106.

[30] Hanley, H.J.M., Meyers, G.J., White, J.W., Sloan, E.D., *Int. J. Thermodyn*. 1989, V.10, 4, 903-909.

[31] Jones, K.W., Kerkar, P.B., Mahajan, D., Kleinberg, R., *Advanced Energy Conference* 2008 "Solution to a global crisis" November 19-20.

[32] Dolliver, M.A., Gresham, T.L., Kistiakowsky, G.B., Smith, E.A., Vaughan, W.E., *J. Am. Chem. Soc*.**,** 1938, 60, 440.

[33] Hayduk, W., Laudie, H.; Smith, O.H., *J. Chem. Eng. Data*, 1973, 18, 373-6.

[34] von Stackelberg, M., *Naturwiss.* 1949, 36, 327, 359.

[35] Cadioli, B., Gallinella, E., Coulombeau, C., Jobic, H., Berthier, G., *J. Phys. Chem.* 1993, *97*, 7844-7856.